

Screening and antiscreening effects in endohedral nanotubes

Pier Luigi Silvestrelli,* Matteo Tessarolo, Abdolvahab Seif, and Alberto
Ambrosetti

Dipartimento di Fisica e Astronomia, Università degli Studi di Padova, 35131 Padova, Italy

E-mail: pierluigi.silvestrelli@unipd.it

Abstract

Recently we investigated from first principles screening properties in systems where small molecules, characterized by a finite electronic dipole moment, are encapsulated into different nanocages. The most relevant result was the observation of an antiscreening effect in alkali-halide nanocages characterized by ionic bonds: in fact, due to the relative displacement of positive and negative ions, induced by the dipole moment of the encapsulated molecule, these cages act as dipole-field amplifiers, differently from what observed in carbon fullerene nanocages, which exhibit instead a pronounced screening effect. Here we extend the study to another class of nanostructures, the nanotubes. Using first-principles techniques based on the Density Functional Theory, we studied the properties of endohedral nanotubes obtained by encapsulation of a water molecule or a linear HF molecule. A detailed analysis of the effective dipole moment of the complexes and of the electronic charge distribution suggests that screening effects crucially depend not only on the nature of the intramolecular bonds but also on the size and the shape of the nanotubes, and on the specific encapsulated molecule. As observed in endohedral nanocages, screening is maximum in covalent-bond carbon nanotubes, while it is reduced in partially-ionic nanotubes and an antiscreening effect is observed in some ionic nanotubes. However in this case the scenario is more complex than in corresponding ionic nanocages. In fact the specific geometric structure of alkali-halide nanotubes turns out to be crucial for determining the screening/antiscreening behavior: while nanotubes with *octagonal* transversal section can exhibit an antiscreening effect, which quantitatively depends on the number of layers in the longitudinal direction, instead nanotubes with *dodecagonal* section are always characterized by a reduction of the total dipole moment, so that a screening behavior is observed. Our results therefore show that, even in nanotube structures, in principle one can tune the dipole moment and generate electrostatic fields at the nanoscale without the aid of external potentials.

Introduction

Since the discovery¹ of Buckminsterfullerene (C_{60}) this complex has received intense study, also considering that, although C_{60} is the most stable and the most common naturally occurring fullerene, many other cage-like nanostructures have been obtained and can be hypothesized, by both considering different numbers of carbon atoms and also replacing carbons with other atoms. Interestingly, by high-energy collisions of ionized fullerene species, harsh conditions of high temperature and pressure, electric arc, or by organic synthesis methods (“molecular surgery”), it is nowadays possible to produce C_{60} endohedral complexes with metal ions, noble gases, and small molecules, such as H_2 , N_2 , H_2O , and CH_4 (the first organic molecule to be encapsulated).²⁻⁸ Such recent achievements in the synthesis of endohedral fullerene complexes have stimulated many experimental and theoretical investigations since the cavity inside fullerenes provides a unique environment for the study of isolated atoms and molecules. Moreover, these systems represent ideal models to study how confinement effects can induce changes in structural and electronic properties of small molecular species and also provide a possible way to alter the properties of the otherwise rather inert fullerenes. In particular, Kurotobi and Murata developed a synthetic route to surgically insert a single water molecule into the most common fullerene C_{60} .⁵ In this case the water molecule, with its relatively large dipole moment (1.8 D), is expected to polarize the symmetric non-polar C_{60} cage. This was confirmed by theoretical first-principles studies⁹⁻¹¹ showing that the dipole moment of $H_2O@C_{60}$ is much lower (about 0.5 D) than that for the isolated water, thus suggesting that a substantial counteracting dipole moment is induced in the C_{60} cage, which considerably screens the electric field produced by the dipole moment of the encapsulated water molecule.

In a recent paper¹² we have investigated endohedral nanocages, characterized by different interatomic interactions, also considering other encapsulated molecules than water. Our calculations of binding and electronic properties, and detailed analysis of the effective dipole moment of the complexes and the electronic charge distribution elucidated the encapsulation

effects and suggest that the screening phenomenon crucially depends on the nature of the intramolecular bonds of the cage: screening is maximum in covalent-bond carbon nanocages, is reduced in partially-ionic ones, while in the case of the ionic-bond nanocages (i.e. $\text{Li}_{36}\text{F}_{36}$) an *antiscreening* effect is observed. Hence, the latter systems surprisingly act as dipole-field amplifiers.

Here we extend the study to different nanotubes: metal carbon nanotubes, partially ionic nanotubes (with alternate B and N, or Be and O, or Ga and N atoms), and ionic, alkali-halide nanotubes. Alkali-halide nanotubes are currently investigated both experimentally and theoretically, particularly focusing on LiF nanotubes because these nanostructures can be obtained experimentally by the impact of fast ions on a LiF polycrystal.¹³⁻¹⁵ On the basis of a relative-stability analysis,¹³ the most stable LiF nanotube structures (and the most suitable for being experimentally realised) turns out to be characterized by *hexagonal* and *octagonal* bases: these structures exhibit a stability similar or higher than that of corresponding cubic clusters.¹³ In particular, first-principles simulations showed¹³ that a LiF nanotube with octagonal base and 7 layers is stable at room temperature and atmospheric pressure. Therefore, since nanotubes with hexagonal section are expected to be too small to allow encapsulation of small molecules, we consider, as a reference alkali-halide system the $\text{Li}_{24}\text{F}_{24}$ nanotube made up of 24 LiF pairs, with *octagonal* base and six layers, although we have subsequently investigated also LiF nanotubes with *dodecagonal* section.

After a preliminary evaluation of the thermal stability of several nanotubes, characterized by intermolecular bonds of different nature, we focus on the properties of the most stable structures. In particular, by considering different binary combinations of alkali metals and halides, we confirm that structures made up of lithium and fluorine atoms are the most stable alkali-halide nanotubes. Previous first-principles calculations showed indeed the high stability of alkali-halide LiF nanotubes¹³ and stable nanotube structures were also found for NaCl and KBr.

Using first-principles techniques based on the Density Functional Theory (DFT), we then

studied the properties of a number of endohedral nanotubes obtained by encapsulation of a water molecule or a linear HF molecule. Similarly to nanocages, also in nanotubes the screening effects crucially depend on the nature of the intramolecular bonds: screening is maximum in covalent-bond carbon nanotubes, while it is reduced in partially-ionic nanotubes and an antiscreening effect is observed in some ionic nanotubes. However in this case the scenario is more complex since screening effects also depend on the size and the shape of the nanotubes. In particular, the specific geometric structure of alkali-halide, ionic nanotubes turns out to be crucial for determining the screening/antiscreening behavior. In fact, while nanotubes with *octagonal* transversal section can exhibit an antiscreening effect, which quantitatively depends on the number of layers in the longitudinal direction, instead nanotubes with *dodecagonal* section are always characterized by a reduction of the total dipole moment, so that a screening behavior is observed. The antiscreening effect in octagonal nanotubes is particularly pronounced for the encapsulated water molecule or the HF-H₂O chained complex, characterized by the formation of Hydrogen bonds. A possible explanation of this intriguing behavior is proposed on the basis of a detailed structural and electronic analysis.

Method

We denote the investigated endohedral complexes as X@Y, where X=HF or H₂O or HF-H₂O, while Y = C_n ($n = 96, 120$) or B₄₈N₄₈ or Be₄₈O₄₈ or Ga₄₈N₄₈ or Li_nF_n ($n = 20, 24, 28, 30, 36, 42$). Nanotubes are characterized not only by the number and type of constituent atoms, but also by their transversal section and the number of layers in the longitudinal direction. For instance, one of the most interesting system in this study is represented by the H₂O@Li₂₄F₂₄*oct-6* structure (see Figure 1), namely a lithium fluoride octagonal nanotube made up of six layers encapsulating a water molecule. Smaller alkali-halide nanotubes, such as Li₁₈F₁₈, turn out to be too small to encapsulate even the simple HF molecule: in fact the HF@Li₁₈F₁₈*oct-6*

endohedral complex is unstable and the nanotube structure is deformed. The same happens if one tries to encapsulate larger molecules, such as LiF, inside the $\text{Li}_{24}\text{F}_{24} \textit{oct-6}$ nanotube. In the case of carbon nanotubes we considered both a C_{96} (4,4) and a C_{120} (5,5) metallic, “armchair” structure.

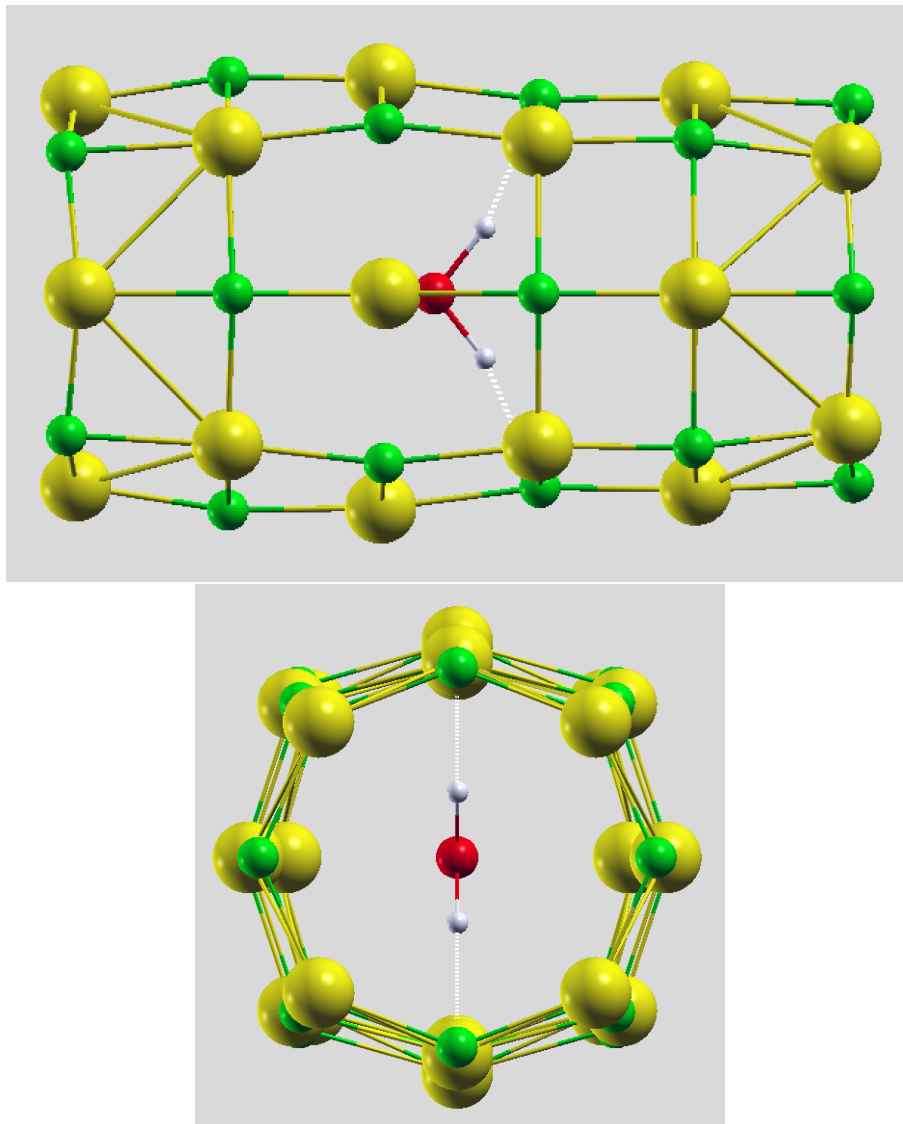


Figure 1: $\text{H}_2\text{O}@\text{Li}_{24}\text{F}_{24} \textit{oct-6}$ endohedral nanostructure. Longitudinal (upper part) and transversal (lower part) view. Yellow, green, red, and white balls represent Li, F, O, and H atoms, respectively. White dashed lines indicate Hydrogen bonds.

Our first-principles simulations have been performed with the Quantum-ESPRESSO *ab initio* package,¹⁶ within the framework of the DFT. In order to simulate endohedral structures

made up of isolated nanotubes, we adopted a tetragonal simulation supercell with periodic boundary conditions. The axis of the nanotube coincides with the z direction of the supercell. This lattice structure was chosen to optimize the ratio between the volume occupied by the structure and the total volume of the supercell. The size of supercell has been the subject of a detailed convergence study to find the best compromise between the computational effort and the accuracy of the results, considering that it must be sufficiently large to avoid significant spurious interactions due to periodic replicas. For our calculations the ratio of c , the dimension along z , and a , the dimension along x and y , of the supercell was kept constant and equal to 2 to match the typical size of the nanotubes, with a ranging from 12 to 15 Å.

The sampling of the Brillouin Zone was restricted to the Γ -point only, which is appropriate for the study of isolated nanostructures. Electron-ion interactions were described using ultrasoft pseudopotentials and the wavefunctions were expanded in a plane-wave basis set with an energy cutoff of 70 Ry. Since van der Waals (vdW) forces are expected to play an important role in the interaction of an encapsulated molecule with the surrounding nanotube,^{11,12} the calculations were performed by adopting the rVV10 DFT functional¹⁷ (the revised, more efficient version of the original VV10 scheme¹⁸), where vdW effects are included by introducing an explicitly nonlocal correlation functional. rVV10 has been found to perform well in many systems and phenomena where vdW effects are relevant, including several adsorption processes.^{17,19,20} In order to elucidate the specific effects of vdW corrections, in some cases binding energies were also computed by replacing the rVV10 DFT functional with the PBE²¹ one, which is a functional unable to properly describe vdW effects. The approach used to accurately describe the screening/antiscreening effect is similar to that adopted in ref.¹² It basically consists in the evaluation of the dipole moment from the valence electron density distribution and the nuclei positions, in the analysis of the differential charge density, and, for ionic nanostructures, in the calculation of the displacements of positive and negative ions of the nanotube upon encapsulation of a small molecule. The electronic dipole moment

of the systems is computed as:

$$\mu = -e \int d\mathbf{r} \mathbf{r} n(\mathbf{r}) + \sum_i^N Z_i e \mathbf{R}_i, \quad (1)$$

where $-e$ is the electron charge, $n(\mathbf{r})$ the electronic number density, and Z_i and \mathbf{R}_i are the valence and spatial coordinate of the i -th ion of the system, respectively.

Results

Preliminary stability tests for several nanotubes were performed considering both their cohesive energy and thermal stability. The cohesive energy (per atom) is defined as:

$$E_c = \left(E - \sum_i^N E_i \right) / N, \quad (2)$$

where E is the total energy of the system, E_i is the energy of the isolated i -th atom, and N is the total number of atoms of the system.

Table 1: Diameter d , cohesive energy E_c , energy gap E_g , and Lindemann number L (at 300 K) of different nanotubes (see text). *oct-6* and *dod-6* denote octagonal or dodecagonal transversal section with 6 layers. For comparison, data relative to selected nanocage structures are also reported.¹²

system	d (Å)	E_c (eV)	E_g (eV)	L
C ₉₆ (4,4)	5.53	-7.98	0.14	0.019
C ₁₂₀ (5,5)	6.83	-8.06	0.05	0.018
B ₄₈ N ₄₈ (4,4)	5.52	-6.36	3.92	0.019
Be ₄₈ O ₄₈ (4,4)	5.71	-6.16	4.87	0.025
Ga ₄₈ N ₄₈ (4,4)	7.05	-3.59	1.50	0.021
Li ₂₄ F ₂₄ <i>oct-6</i>	4.90	-4.23	6.40	0.053
Li ₃₆ F ₃₆ <i>dod-6</i>	7.38	-4.23	6.07	0.064
C ₆₀ nanocage	7.10	-7.92	1.65	0.017
B ₃₆ N ₃₆ nanocage	8.70	-7.65	4.48	0.019
Be ₃₆ O ₃₆ nanocage	8.03	-6.09	4.89	0.024
Si ₆₀ nanocage	11.67	-3.86	0.39	0.100
Li ₃₆ F ₃₆ nanocage	9.36	-4.16	5.86	0.050

As can be seen in Table I, the cohesive energies and energy gaps of the considered nanotubes are similar to those of nanocages made up of the same constituent atoms. In particular, the cohesive energy of the LiF nanotubes is slightly larger (in absolute value) than that of the $\text{Li}_{36}\text{F}_{36}$ nanocage investigated in ref.¹²

As far as the thermal stability is concerned, the Lindemann parameter, widely used for determining the melting temperatures of bulk solids is not appropriate for application to nanotubes.^{22,23} Instead, a modified Lindemann number L , based on nearest-neighbor distance fluctuations, turns out to be effective:²³

$$L = \frac{1}{N_1} \sum_{i,j=1,N_1} \frac{\sqrt{\langle r_{ij}^2 \rangle - \langle r_{ij} \rangle^2}}{\langle r_{ij} \rangle} \quad (3)$$

where N_1 is the number of all nearest-neighbor atom pairs, r_{ij} is the modulus of the difference vector between nearest-neighbor atoms, and $\langle \dots \rangle$ denotes average over the Molecular Dynamics (MD) simulation steps. In the present study MD simulations were performed, at different temperatures, using the Verlet algorithm to integrate the equations of motion, with a time step of 0.968 fs and a total simulation time of about 9.7 ps. The temperature was controlled by the velocity scaling method. Below the melting temperature L is expected to increase slowly and linearly with temperature, due to the stable constraint of the atomic potentials and the linear increase in the kinetic energy, just reflecting atomic thermal vibrations around the original positions; instead above the melting temperature L is more sensitive to the temperature change and deviate from linear behaviour by exhibiting an abrupt increase.^{22,23} At the melting temperature L should be characterized by a value of the order of 0.050.^{22,23}

As expected, estimated L values of Table I indicate that the thermal stability of carbon and partially ionic nanotubes at room temperature is higher than that of ionic nanotubes, in line with the behavior observed in the cohesive energy and in the corresponding nanocages. By comparing L in LiF nanotubes one can see that the thermal stability of the $\text{Li}_{24}\text{F}_{24}$ *oct-6*

is slightly higher than that of $\text{Li}_{36}\text{F}_{36}$ *dod-6* although the cohesive energies of the two systems are essentially equal.

In Table II we report the basic properties of endohedral complexes made up of H_2O and HF molecules encapsulated inside the selected nanotubes. Extensive calculations indicate that in any case the most favored configuration is typically represented (see, for example, $\text{H}_2\text{O}@\text{Li}_{24}\text{F}_{24}$ *oct-6* in Figure 1) by the encapsulated molecule located in a central positions inside the nanotubes with its dipole moment parallel to the axis of the nanostructure. In some endohedral structures ($\text{H}_2\text{O}@\text{B}_{48}\text{N}_{48}$ (4,4), $\text{H}_2\text{O}@\text{Be}_{48}\text{O}_{48}$ (4,4), $\text{H}_2\text{O}@\text{Li}_{24}\text{F}_{24}$ *oct-6*, and $\text{H}_2\text{O}@\text{Li}_{36}\text{F}_{36}$ *dod-6*) the encapsulated water molecule forms 2 Hydrogen bonds with, respectively, the N, O, F atoms of the surrounding nanotube.

The binding energies (in meV, 1 kJ/mol=10.36 meV, 1 kcal/mol=43.36 meV) of endohedral systems are computed as the difference between the total energy of the X@Y complex and the sum of the total energies of the constituent parts X and Y:

$$E_{\text{bind}} = E(\text{X@Y}) - E(\text{X}) - E(\text{Y}) . \quad (4)$$

In some cases we also report the binding energies obtained by replacing the rVV10 DFT functional with the PBE one, so without properly taking vdW interactions into account. Note that in the present systems zero-point energy (ZPE) effects are expected to be small: in fact Dolgonos and Peslherbe²⁴ verified that the stability of endohedral complexes is not considerably affected by ZPE correction of the interaction energies, which does not exceed 10%. Clearly a negative value of the binding energy indicates that the molecule energetically prefers to be encapsulated inside the nanotube rather than being isolated, although an energy barrier may have to be overcome to penetrate the nanotube (see detailed discussion below). In a few cases ($\text{H}_2\text{O}@\text{C}_{96}$ (4,4), $\text{HF}@\text{C}_{96}$ (4,4), $\text{HF}@\text{B}_{48}\text{N}_{48}$ (4,4)) the computed binding energy is positive, thus suggesting that the configuration with the encapsulated molecule is unfavored. Note that, in the case of carbon nanotubes, while the binding energy is positive

for the molecules inside C_{96} (4,4) with a diameter of $d = 5.53 \text{ \AA}$, it becomes negative considering the larger C_{120} (5,5) nanotube (diameter of $d = 6.83 \text{ \AA}$). As can be seen, similarly to what found in endohedral nanocages,¹² the binding energy of the encapsulated molecules is mostly due to vdW interactions; in fact using the PBE functional (unable to reproduce vdW effects) the binding energy is much reduced (in absolute value) and becomes even positive in $H_2O@Li_{24}F_{24}oct-6$ and $HF@Li_{24}F_{24}oct-6$.

All the considered nanotubes, in their optimized, isolated structure, are characterized by a negligible total dipole moment (in all cases not larger than 0.1 D, with the exception of the $Be_{48}O_{48}$ (4,4) nanotube with a moderate dipole moment of 0.26 D along the longitudinal axis). The scenario changes when a small molecule with a finite electronic dipole moment is encapsulated into the nanotubes, as can be seen in Table II where we report both the total dipole moment of the endohedral complexes and the change (in absolute value and in percentage) of the dipole moment with respect to that of the isolated H_2O or HF molecule, due to the presence of the surrounding nanotube. Remarkably, in the investigated C nanotubes the screening effect is almost total (more than 90%), being even more pronounced than that observed in C nanocages.¹² In partially-ionic nanotubes the screening effect is instead intermediate and comparable to that found in the corresponding nanocages,¹² ranging from 16 to 63%.

Interestingly, in the case of the $H_2O@Li_{24}F_{24}oct-6$ and $HF@Li_{24}F_{24}oct-6$ endohedral complexes an evident *antiscreening* effect is detected, with a noticeable dipole amplification. This effect is comparable to that observed in the corresponding LiF alkali-halide nanocage¹² for the encapsulated HF molecule (+16% vs. +20%) and even significantly stronger for the encapsulated water molecule (+35% vs. +18%). In order to find to what extent the rearrangement of the $Li_{24}F_{24}oct-6$ nanotube atoms can induce the dipole amplification we performed constrained relaxations for both $H_2O@Li_{24}F_{24}oct-6$ and $HF@Li_{24}F_{24}oct-6$. If only the z coordinates (those along the nanotube axis and the molecule dipole moment) of the nanotube atoms are allowed to relax, the optimized configurations are energetically unstable

(positive binding energy) and a moderate dipole reduction of the endohedral complexes is observed; so this axial relaxation cannot be the source of the antiscreening effect, at difference from what found in alkali-halide nanocages.¹² Instead configuration stability and antiscreening effect are recovered by just allowing the radial relaxation of the $\text{Li}_{24}\text{F}_{24} \text{ oct-6}$ nanotube (i.e. relaxing x and y atomic coordinates only). As a consequence of the molecule encapsulation the $\text{Li}_{24}\text{F}_{24} \text{ oct-6}$ nanotube undergoes a global *radial expansion*, more pronounced in $\text{H}_2\text{O}@\text{Li}_{24}\text{F}_{24} \text{ oct-6}$ than in $\text{HF}@\text{Li}_{24}\text{F}_{24} \text{ oct-6}$: in particular, the average radial expansion of the Li and F atoms is 3.6 and 2.2 mÅ in $\text{HF}@\text{Li}_{24}\text{F}_{24} \text{ oct-6}$ and 29.0 and 26.3 mÅ in $\text{H}_2\text{O}@\text{Li}_{24}\text{F}_{24} \text{ oct-6}$, this quantitative difference being explained by the larger size of the H_2O molecule than of HF. Also note that the water molecule forms 2 Hydrogen bonds with 2 F atoms of the $\text{Li}_{24}\text{F}_{24} \text{ oct-6}$ nanotube (see Figure 1), which further contributes to the dipole-moment amplification and explains the stronger binding of the H_2O molecule than of HF. In alkali-halide LiF complexes, due to charge redistribution, the Li and F atoms are positively and negatively charged, so they can be considered actually as Li^+ and F^- ions. So, it is just this radial ion rearrangement that produces the antiscreening effect.

However, the size of the alkali-halide nanotube plays a crucial role in determining the screening properties of the alkali-halide nanotubes. In fact, in the case of the $\text{H}_2\text{O}@\text{Li}_{36}\text{F}_{36} \text{ dod-6}$ and $\text{HF}@\text{Li}_{36}\text{F}_{36} \text{ dod-6}$ endohedral complexes, the scenario is different. From one hand the binding energies are again quite similar for H_2O and HF but much larger (in absolute value) than in the corresponding structures with $\text{Li}_{24}\text{F}_{24} \text{ oct-6}$ nanotubes; $\text{H}_2\text{O}@\text{Li}_{36}\text{F}_{36} \text{ dod-6}$ and $\text{HF}@\text{Li}_{36}\text{F}_{36} \text{ dod-6}$ are stable structures even with the PBE functional, so here vdW effects are important but slightly less crucial for structure stabilization. More importantly, here a clear *screening* effect is found, quantitatively similar to that observed (see Table II) in $\text{B}_{48}\text{N}_{48}$ (4,4), $\text{Be}_{48}\text{O}_{48}$ (4,4), and $\text{Ga}_{48}\text{N}_{48}$ (4,4) partially ionic nanotubes. In fact there is a significant dipole reduction, which is more pronounced in $\text{H}_2\text{O}@\text{Li}_{36}\text{F}_{36} \text{ dod-6}$. Differently from what happens for the $\text{Li}_{24}\text{F}_{24} \text{ oct-6}$ nanotube, in this case a significant radial contraction is observed upon encapsulation of a small molecule: the average radial contraction of

the Li and F atoms is 192.3 and 198.3 mÅ in $\text{HF}@Li_{36}F_{36}dod-6$ and 32.4 and 34.6 mÅ in $\text{H}_2\text{O}@Li_{36}F_{36}dod-6$ (see Figure 2). Here the screening effect is recovered by just relaxing the z coordinates of the nanotube atoms.

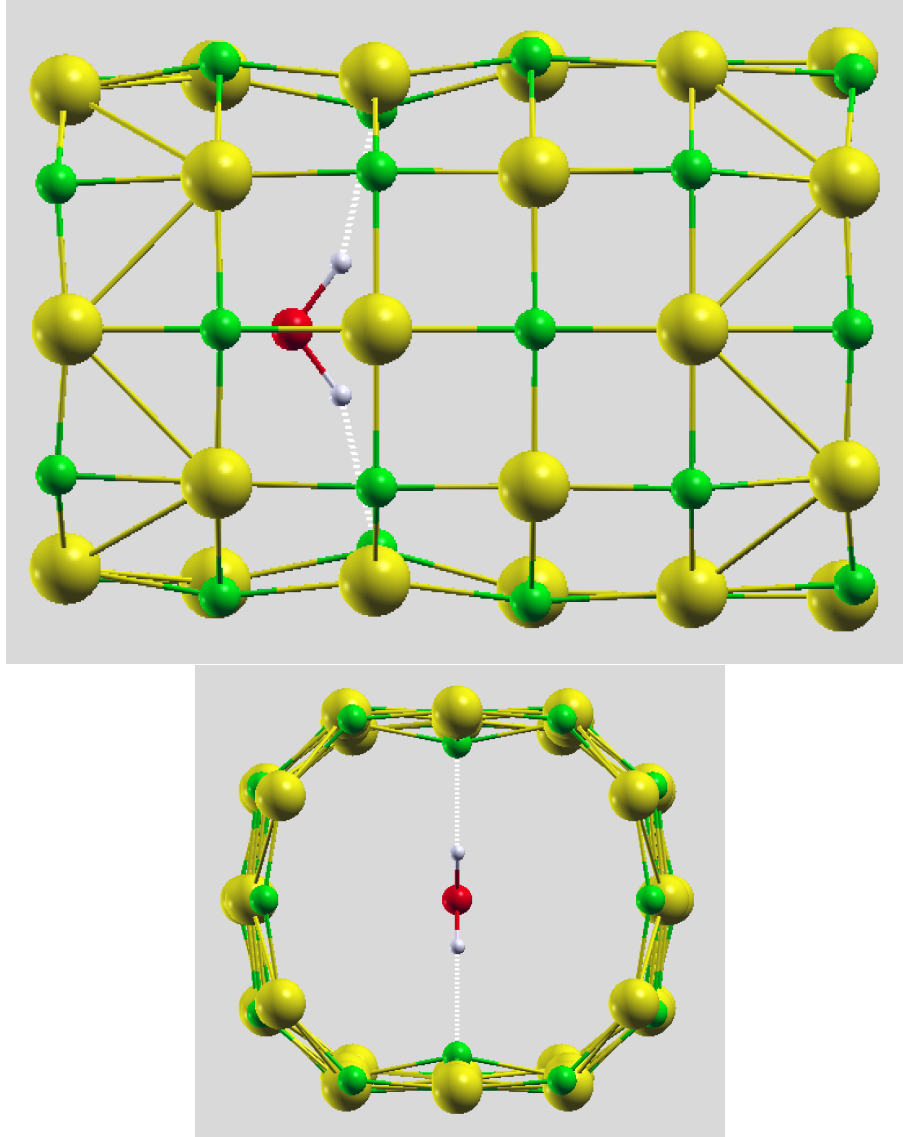


Figure 2: $\text{H}_2\text{O}@Li_{36}F_{36}dod-6$ endohedral nanostructure. Longitudinal (upper part) and transversal (lower part) view. Yellow, green, red, and white balls represent Li, F, O, and H atoms, respectively. White dashed lines indicate Hydrogen bonds.

So, basically, radial atomic displacements appear to be the main source of the antiscreening effect in $\text{Li}_{24}\text{F}_{24}oct-6$, while longitudinal ones (along the z coordinate) are the main source of screening in $\text{Li}_{36}\text{F}_{36}dod-6$. We also note that, upon encapsulation, the $\text{Li}_{36}\text{F}_{36}dod-6$

nanotube is significantly more deformed than $\text{Li}_{24}\text{F}_{24} \text{ oct-6}$ (see Figure 2). This effect can be made quantitative by estimating the *eccentricity* of the nanostructures, which can be defined as

$$e = \sqrt{1 - (R_2/R_1)^2} \quad (5)$$

where R_1 and R_2 are the largest and the smallest nanotube radius, respectively. The computed e values are 0.08 and 0.27 for $\text{HF}@\text{Li}_{24}\text{F}_{24} \text{ oct-6}$ and $\text{H}_2\text{O}@\text{Li}_{24}\text{F}_{24} \text{ oct-6}$, to be compared to the e values of 0.65 and 0.80 for $\text{HF}@\text{Li}_{36}\text{F}_{36} \text{ dod-6}$ and $\text{H}_2\text{O}@\text{Li}_{36}\text{F}_{36} \text{ dod-6}$.

In order to better elucidate the mechanisms underlying the dipole-moment variations in endohedral nanotubes, a further analysis is performed by focusing on the electron-density variations. In Figures 3-5 we show the changes in the electron distribution, for the $\text{H}_2\text{O}@\text{C}_{120} (5,5)$, $\text{H}_2\text{O}@\text{Li}_{24}\text{F}_{24} \text{ oct-6}$, and $\text{H}_2\text{O}@\text{Li}_{36}\text{F}_{36} \text{ dod-6}$ systems, resulting from the encapsulation processes. The plotted differential charge density, $\delta\rho$, is defined as the difference between the total electron density of the whole system and the superposition of the densities of the separated fragments (H_2O molecule and nanotube), keeping the same geometrical structure and atomic positions that these fragments have within the whole optimized system.

In Figures 6-8 we also plot the one-dimensional profiles $\delta\rho(z)$, computed along the nanotube z axis, as a function of z -coordinate values, by integrating $\delta\rho$ over the corresponding, orthogonal x,y planes.

As can be seen in Figure 3, in $\text{H}_2\text{O}@\text{C}_{120} (5,5)$ there is a pronounced electron charge accumulation in the region between the H atoms and the nanotube and a corresponding charge depletion around the O atom leading to the formation of the counteracting dipole moment which considerably reduces the effective dipole moment of the endohedral complex; clearly the overall response of the $\text{C}_{120} (5,5)$ nanotube to the H_2O molecule dipole moment is a significant charge density shift. One can make more quantitative the information contained in Figure 6 by evaluating the induced dipole moment as: $\mu_{\text{ind}} = - \int dz z \delta\rho(z)$, where $\delta\rho(z)$ has been defined above. The numerical value of $\mu_{\text{ind}} = 1.65$ D is found to coincide (see Figure

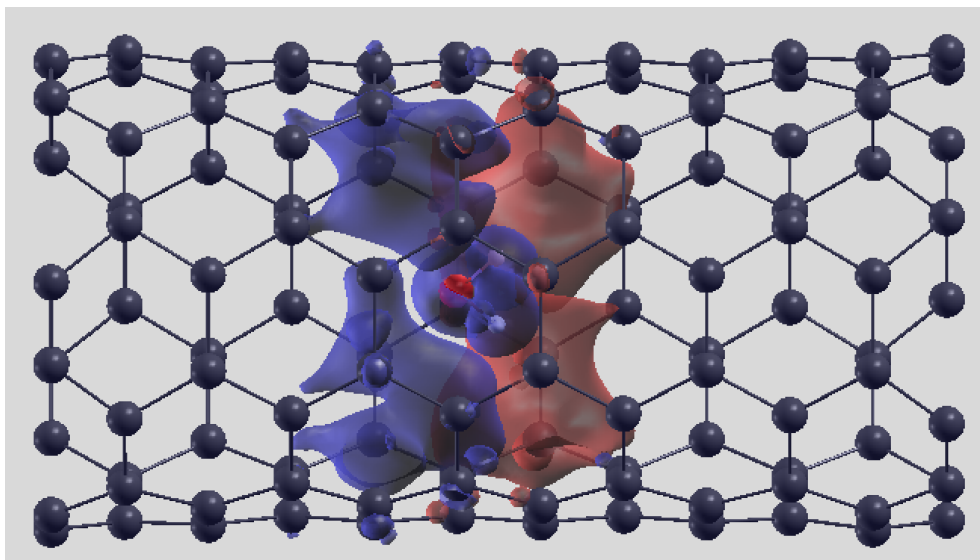


Figure 3: Differential electron charge density, $\Delta\rho$, for $\text{H}_2\text{O}@C_{120}$ (5,5), with isosurfaces shown at $\pm 2 \times 10^{-3} e/\text{\AA}^3$. Red areas indicate electron density gain, while blue areas indicate loss of electron density relative to the empty C_{120} (5,5) nanotube and the isolated H_2O molecule.

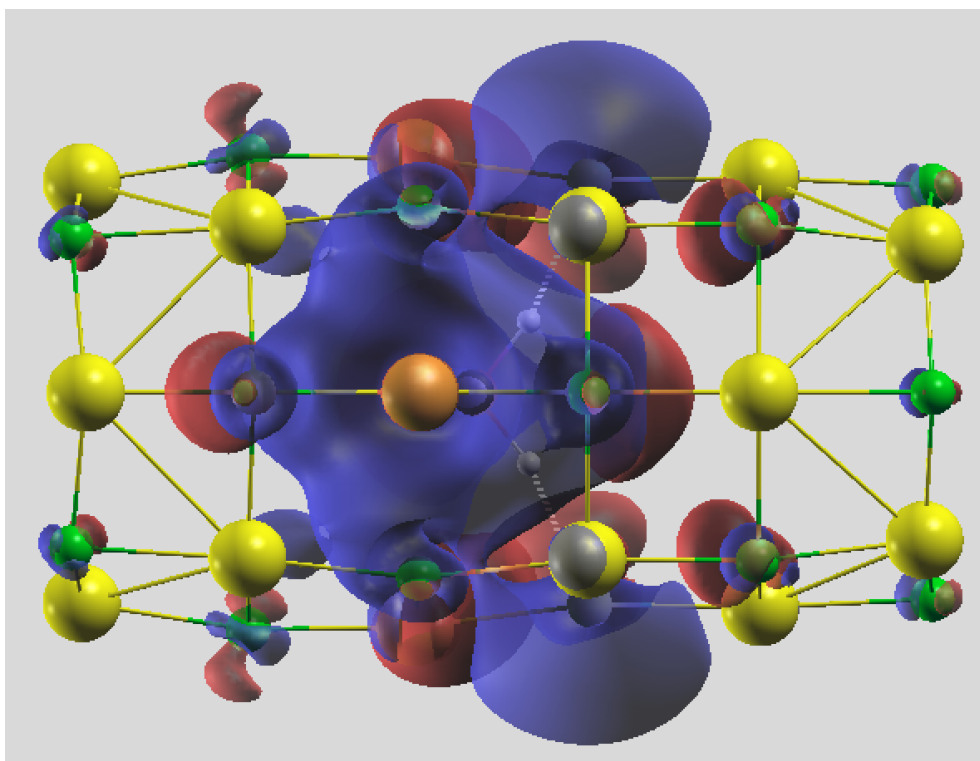


Figure 4: Differential electron charge density, $\Delta\rho$, for $\text{H}_2\text{O}@Li_{24}F_{24} \text{ oct-6}$, with isosurfaces shown at $\pm 2 \times 10^{-3} e/\text{\AA}^3$. Red areas indicate electron density gain, while blue areas indicate loss of electron density relative to the empty $Li_{24}F_{24} \text{ oct-6}$ nanotube and the isolated H_2O molecule.

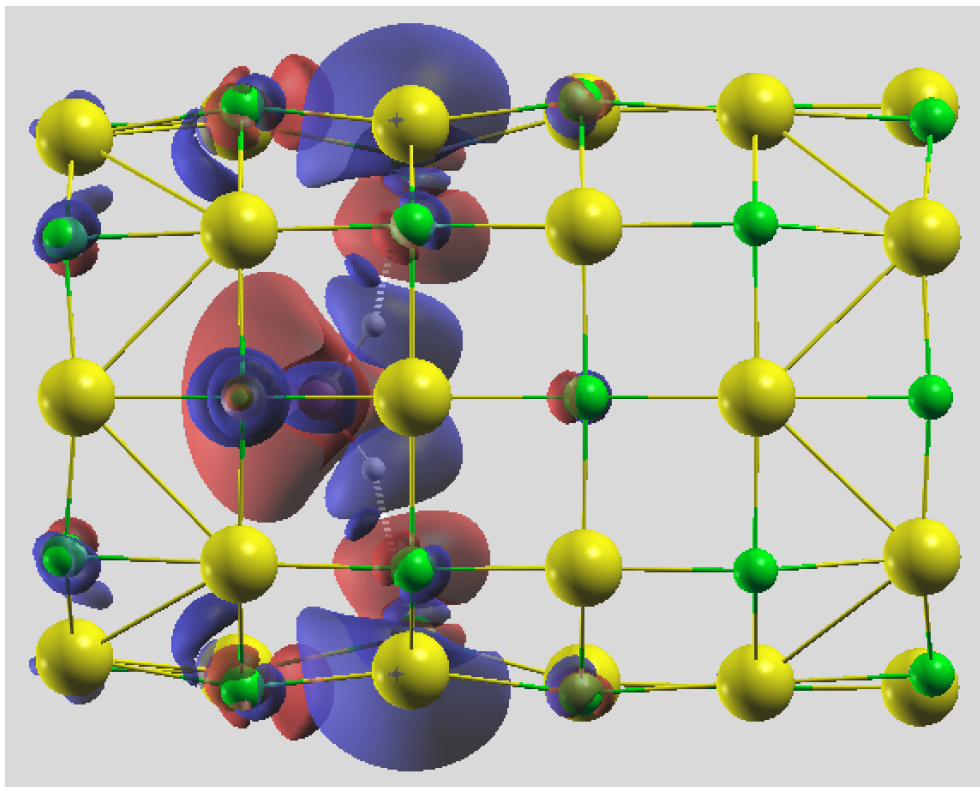


Figure 5: Differential electron charge density, $\Delta\rho$, for $\text{H}_2\text{O}@\text{Li}_{36}\text{F}_{36}\text{dod-6}$, with isosurfaces shown at $\pm 2 \times 10^{-3} e/\text{\AA}^3$. Red areas indicate electron density gain, while blue areas indicate loss of electron density relative to the empty $\text{Li}_{36}\text{F}_{36}\text{dod-6}$ nanotube and the isolated H_2O molecule.

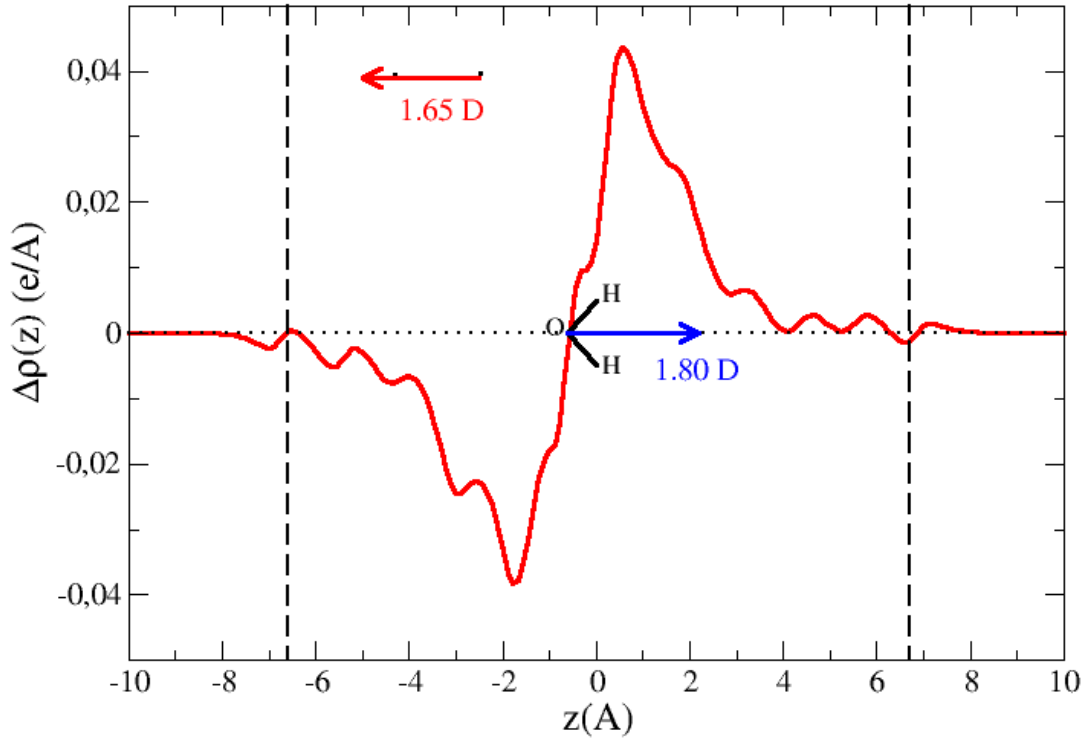


Figure 6: Differential electron charge density, $\Delta\rho(z)$, along the nanotube z axis, in $\text{H}_2\text{O}@\text{C}_{120}-(5,5)$. The vertical, black, dashed lines indicate the boundaries of the nanotube, while the red arrow represents the induced dipole moment with a numerical value obtained by integration on the z axis (see text). The dipole moment of the water molecule is also reported in blue.

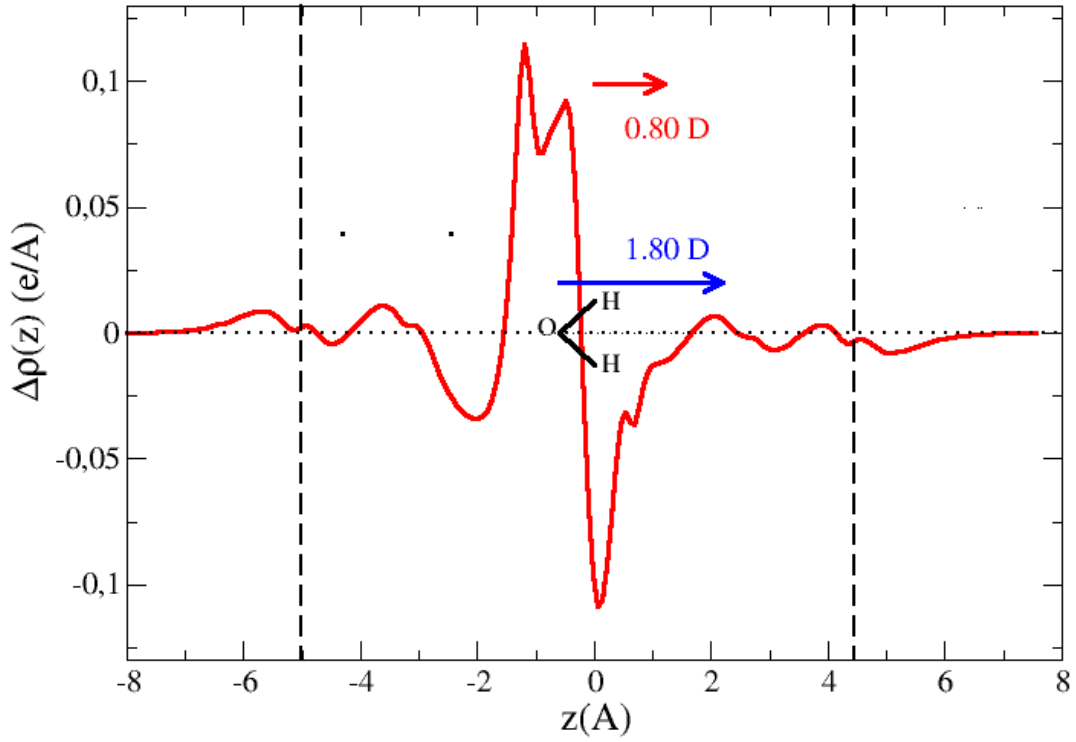


Figure 7: Differential electron charge density, $\Delta\rho(z)$, along the nanotube z axis, in $\text{H}_2\text{O}@Li_{24}F_{24}oct-6$. The vertical, black, dashed lines indicate the boundaries of the nanotube, while the red arrow represents the induced dipole moment with a numerical value obtained by integration on the z axis (see text). The dipole moment of the water molecule is also reported in blue.

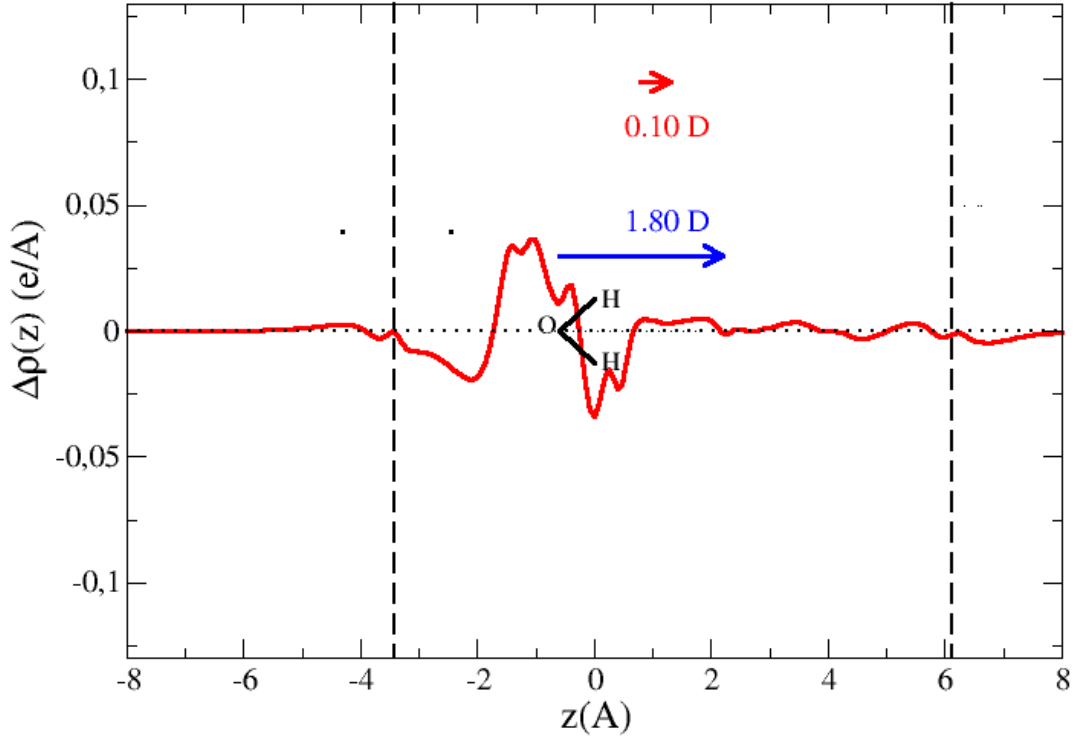


Figure 8: Differential electron charge density, $\Delta\rho(z)$, along the nanotube z axis, in $\text{H}_2\text{O}@Li_{36}F_{36}dod-6$. The vertical, black, dashed lines indicate the boundaries of the nanotube, while the red arrow represents the induced dipole moment with a numerical value obtained by integration on the z axis (see text). The dipole moment of the water molecule is also reported in blue.

6) with that of $\delta\mu$ reported in Table II.

In ionic nanotubes the situation is more complex. Considering $\text{H}_2\text{O}@\text{Li}_{24}\text{F}_{24}\text{oct-6}$, one can see (Figure 4) that the regions where the differential charge density is mostly localized are in the center of the nanotube, around the O atom of the water molecule, and also in close vicinity of the 2 H atoms facing 2 F atoms of the nanotube. In Figure 7 we plot $\delta\rho(z)$. The corresponding induced dipole moment, $\mu_{\text{ind}} = 0.17$ D, is due to the rearranged electron density. One can therefore conclude that, for this system, the dipole-amplification (antiscreening) effect ($\delta\mu = +0.63$ D, see Table II) is due, for about 30% to the deformation of the electronic cloud, while the remaining portion is due to the relative displacements of positive and negative ions. In fact the water molecule encapsulated inside the nanotube interacts with the positive and negative ions, slightly distorting the nanostructure, with the formation of 2 Hydrogen bonds too, as discussed above. This effect contributes significantly to the amplified electric dipole moment. In order to better characterize these distortions one can consider z_+ , that is the z component of the charge center of the positive ions Li^+ , and z_- , the z component of the charge center of the negative ions F^- ; then one can evaluate $d_{\pm} = z_+ - z_-$, that is the difference between the z -coordinates of the charge centers of the positive and negative ions (d_{\pm} is conveniently expressed in $\text{m}\text{\AA}$ being a very small quantity). As expected, d_{\pm} increases significantly upon water-molecule encapsulation (1.7 $\text{m}\text{\AA}$) from the value computed in the isolated $\text{Li}_{24}\text{F}_{24}\text{oct-6}$ nanotube (0.7 $\text{m}\text{\AA}$). A more detailed description can be obtained (similarly to what done in ref.¹²) by plotting the z -coordinate changes of the ions, upon encapsulation of the water molecule, as a function of the z position of the ions themselves. Since each transversal section of the $\text{Li}_{24}\text{F}_{24}\text{oct-6}$ nanotube has 8 alternating ions (4 Li^+ and 4 F^- ions) we consider the average position along z of each of the two sets of 4 ions: z_{+i} for the 4 Li^+ ions and z_{-i} for the 4 F^- ions of the i -th section. Figure 9 shows the behavior of z_{+i} and z_{-i} in the $\text{Li}_{24}\text{F}_{24}\text{oct-6}$ nanotube (the dotted lines are just a guide to the eyes).

Interestingly, lithium-fluoride endohedral structures with the dodecagonal section, differ-

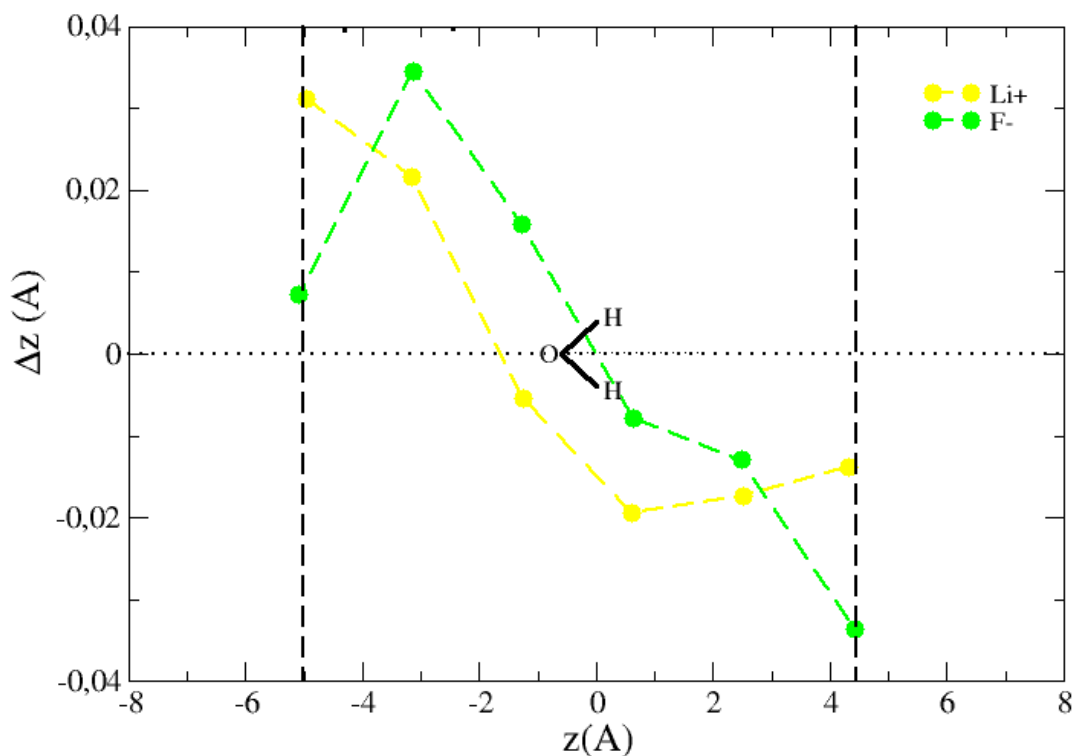


Figure 9: $\text{H}_2\text{O}@\text{Li}_{24}\text{F}_{24}\text{oct-6}$ endohedral complex: displacements, along the nanotube z axis, of Li^+ and F^- ions of the $\text{Li}_{24}\text{F}_{24}\text{oct-6}$ ionic nanotube upon encapsulation of H_2O : small circles represent the actual displacements of the ions, while the dashed lines are just a guide for the eye. The vertical, black, dashed lines indicate the positions of the nanotube boundaries.

ently from those with the octagonal one, exhibit a clear screening effect since the total-dipole moment is reduced with respect to that of the isolated molecules (see Table II). As can be seen in Figure 2, the endohedral $\text{H}_2\text{O}@Li_{36}F_{36}dod-6$ structure is characterized by a significant deformation in the transversal direction (see also the above discussion) with the water molecule that forms 2 Hydrogen bonds with 2 F atoms of the nanotube in this case too. The differential charge density $\delta\rho$ of $\text{H}_2\text{O}@Li_{36}F_{36}dod-6$ is plotted in Figure 5. A clear difference is evident with respect to the $\delta\rho$ distribution in $\text{H}_2\text{O}@Li_{24}F_{24}oct-6$: the electronic charge variations are much smaller (also compare Figure 7 with Figure 8) than those observed in $\text{H}_2\text{O}@Li_{24}F_{24}oct-6$. As a consequence, by integration one obtains a smaller induced dipole moment (see Figure 8) of 0.10 D. However, in this case, the slight increase of the dipole moment is more than compensated by the dipole-moment reduction due to the relative displacements of positive and negative ions, leading to an overall decrease of the the total dipole moment (screening effect). As can be seen in Figure 10, the behavior of these displacements is both qualitatively and quantitatively different from that of the $\text{H}_2\text{O}@Li_{24}F_{24}oct-6$ case. From one hand in $\text{H}_2\text{O}@Li_{24}F_{24}oct-6$ the displacements are almost double than in $\text{H}_2\text{O}@Li_{36}F_{36}dod-6$; from the other in the dodecagonal nanotube case the Li^+ ions displacements are on average smaller than those of the F^- ones, leading to an overall distance between positive and negative ion centers along z of $d_{\pm} = -4.6 \text{ m\AA}$. Such a negative value indicates that in $\text{H}_2\text{O}@Li_{36}F_{36}dod-6$ the ion displacements induce a screening effect, at a difference from $\text{H}_2\text{O}@Li_{24}F_{24}oct-6$, where instead the opposite effect is observed.

The changes in the dipole moment of endohedral LiF nanotubes upon encapsulation of a molecule can also be semiquantitatively reproduced by using a simple electrostatic model, where the Li^+ and F^- ions of the nanotubes are replaced by positive and negative charges ($+0.71 e$ and $-0.71 e$, respectively, where the effective, partial charges were estimated in ref.¹²). The electric field E generated by these charges at the position of the encapsulated molecule gives rise to an induced dipole moment which can be easily evaluated as $\Delta\mu = \alpha E$, where α is the polarizability of the encapsulated molecule, which is assumed to be isotropic (a

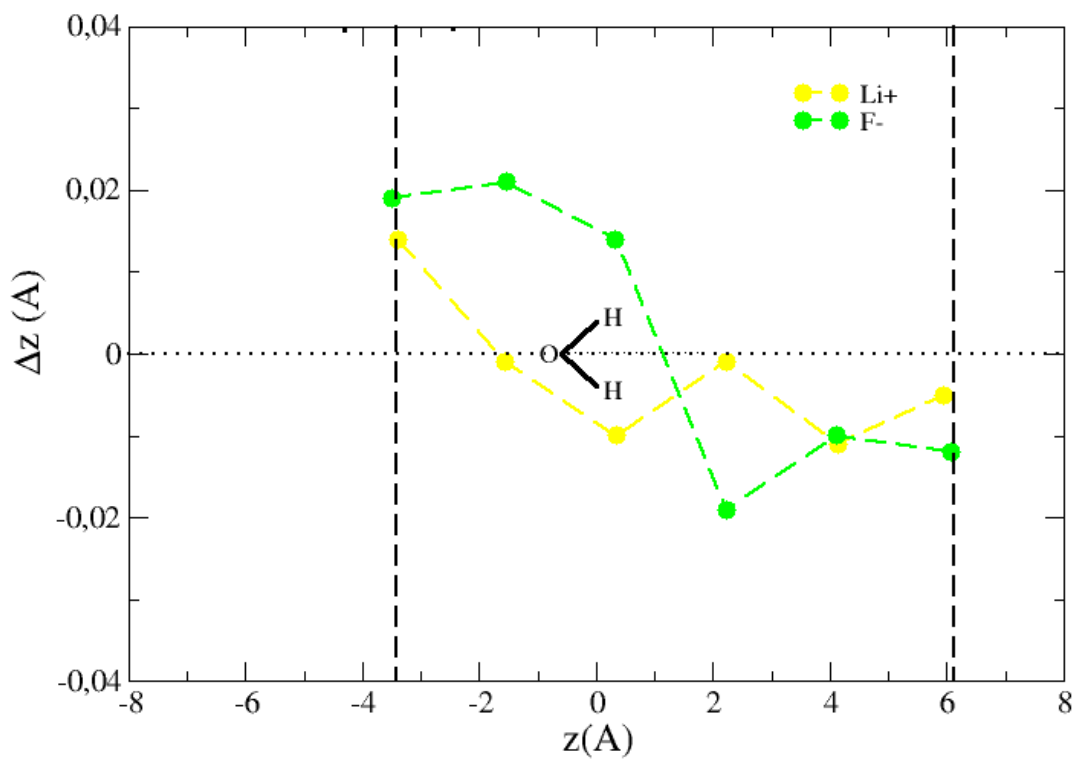


Figure 10: $\text{H}_2\text{O}@\text{Li}_{36}\text{F}_{36}$ *dod-6* endohedral complex: displacements, along the nanotube z axis, of Li^+ and F^- ions of the $\text{Li}_{36}\text{F}_{36}$ *oct-6* ionic nanotube upon encapsulation of H_2O : small circles represent the actual displacements of the ions, while the dashed lines are just a guide for the eye. The vertical, black, dashed lines indicate the positions of the nanotube boundaries.

good approximation for water). Considering the induced dipole moment along the nanotube axis one finds that $\Delta\mu = +0.66$ and $+0.36$ D for $\text{H}_2\text{O}@Li_{24}F_{24} \textit{oct-6}$ and $\text{HF}@Li_{24}F_{24} \textit{oct-6}$, respectively, in reasonable agreement with the corresponding increases of the dipole moments ($+0.63$ and $+0.29$ D) reported in Table II (antiscreening effect). Instead, in $Li_{36}F_{36} \textit{dod-6}$ the relatively small induced dipole moments ($+0.21$ and $+0.03$ D for encapsulated H_2O and HF molecule) are more than compensated by the counteracting dipole moment (-0.57 and -0.50 D) induced in the nanotube, due to the rearrangement of the Li and F atoms, thus leading to an overall reduction of the total dipole moment (screening effect).

We have also verified that, by replacing the rVV10 DFT functional with the PBE one (unable to properly describe the vdW effects) the antiscreening and screening behavior is qualitatively preserved in $Li_{24}F_{24} \textit{oct-6}$ and in $Li_{36}F_{36} \textit{dod-6}$, respectively, in spite of the dramatic reduction of binding of the encapsulated molecules, thus suggesting that vdW interactions do not play a crucial role in determining the screening properties, which are mostly due to electrostatic interactions, as also confirmed by the reasonable description obtained by the simple electrostatic model introduced above.

To assess the effect of changing the number of layers in the selected ionic nanotubes characterized by octagonal or dodecagonal transversal section, we evaluated the dipole moment of the endohedral complexes with encapsulated molecules also in nanotubes with one less ($Li_{20}F_{20} \textit{oct-5}$ and $Li_{30}F_{30} \textit{dod-5}$) and one more layer ($Li_{28}F_{28} \textit{oct-7}$ and $\text{H}_2\text{O}@Li_{42}F_{42} \textit{dod-7}$) than the 6 layers considered so far. As can be seen in Table III, the number of layers plays a significant role in octagonal LiF nanotubes; in fact the antiscreening effect turns out to be maximum for the $Li_{24}F_{24} \textit{oct-6}$ nanotube with 6 layers. In the case of the encapsulated water molecule the dipole amplification is substantially reduced ($+15\%$ vs. $+35\%$) with 5 layers while the reduction is less pronounced ($+31\%$ vs. $+35\%$) with 7 layers. For the encapsulated HF molecule the dependence is even stronger: with 5 and 7 layers a screening effect is observed instead of an antiscreening one, with a decrease of the dipole moment: from $+16\%$ to -21% and from $+16\%$ to -6% with 5 and 7 layers, respectively. Instead in dodecagonal

LiF nanotubes a milder dependence on the number of nanotube layers is found, with the screening behavior which is observed in all the considered cases.

The binding energies of the encapsulated molecules do not vary much with the number of layers (see Table III), but for the $\text{Li}_{42}\text{F}_{42}\text{dod-7}$ nanotube. In fact, in this case E_{bind} is severely reduced (in absolute value). We have verified that this is due to a different geometric structure of the endohedral $\text{H}_2\text{O}@\text{Li}_{42}\text{F}_{42}\text{dod-7}$ and $\text{HF}@\text{Li}_{42}\text{F}_{42}\text{dod-7}$ nanostructures: in fact in these cases the dodecagonal nanotube is more rigid and thus much less distorted upon molecule encapsulation than with 5 or 6 layers, so that the interaction with the inside molecule is much reduced due to an average larger distance from the atoms of the nanotube.

When considering hypothetical endohedral nanostructures it is clearly important to have an estimate of the energy cost required (if any) to encapsulate a given molecule. To this aim we found the optimal reaction path for encapsulation of a single H_2O or HF molecule, from a position outside to the optimal one inside the different considered nanotubes, using the Nudged Elastic Band (NEB) method combined with the climbing-image approach and the quasi-Newton Broyden's second method.²⁵

The energy barriers for the encapsulation of H_2O and HF molecules inside the nanotubes are reported in Table IV. As can be seen, in case of carbon nanotubes, encapsulation requires overcoming an energy barrier of about 0.5 and 0.1 eV in C_{96} (4,4) for H_2O and HF , respectively, while the encapsulation process is instead barrierless in the larger C_{120} (5,5) nanotube. Similarly, in ionic nanotubes the energy barrier is about 0.5 and 0.4 eV in $\text{Li}_{24}\text{F}_{24}\text{oct-6}$ for H_2O and HF , respectively, while encapsulation is barrierless in $\text{Li}_{36}\text{F}_{36}\text{dod-6}$. In partially ionic nanotubes the energy barriers range from about 0.06 and 0.3 eV in $\text{B}_{48}\text{N}_{48}$ (4,4) to much larger values (2.6 and 3.7 eV) in $\text{Be}_{48}\text{O}_{48}$ (4,4).

Interestingly, it is possible to further amplify the dipole moment of the endohedral $\text{Li}_{24}\text{F}_{24}\text{oct-6}$ nanotube by encapsulating multiple molecules. For instance we have verified that when a H_2O and a HF molecule are chained inside the nanotube (Figure 11) the dipole moment of the endohedral structure is 5.14 D, which is a value considerably larger than both

Table 2: Electronic dipole moment (along the nanotube axis) μ of endohedral complexes with H₂O or HF molecule inside; $\delta\mu$ denotes the change of the dipole moment of the endohedral complex with respect to those computed for the encapsulated H₂O and HF molecules when they are isolated (1.80 and 1.79 D, respectively). E_{bind} is the binding energy (in square parenthesis using the PBE functional in place of rVV10) of endohedral complexes. *oct-6* and *dod-6* denote octagonal or dodecagonal transversal section with 6 layers. For comparison we also report corresponding results obtained considering the H₂O and HF molecules encapsulated in selected nanocages.¹²

system	μ (D)	$\delta\mu$ (D)	E_{bind} (meV)
H ₂ O@C ₉₆ (4,4)	0.07	-1.74 (-96%)	+460
HF@C ₉₆ (4,4)	0.09	-1.69 (-95%)	+101
H ₂ O@C ₁₂₀ (5,5)	0.15	-1.65 (-92%)	-442
HF@C ₁₂₀ (5,5)	0.14	-1.64 (-92%)	-332
H ₂ O@B ₄₈ N ₄₈ (4,4)	1.20	-0.60 (-34%)	-554
HF@B ₄₈ N ₄₈ (4,4)	1.06	-0.72 (-40%)	+47
H ₂ O@Be ₄₈ O ₄₈ (4,4)	1.52	-0.29 (-16%)	-195
HF@Be ₄₈ O ₄₈ (4,4)	1.12	-0.66 (-37%)	-165
H ₂ O@Ga ₄₈ N ₄₈ (4,4)	0.67	-1.12 (-63%)	-290
HF@Ga ₄₈ N ₄₈ (4,4)	0.71	-1.09 (-60%)	-403
H ₂ O@Li ₂₄ F ₂₄ <i>oct-6</i>	2.43	+0.63 (+35%)	-230[+302]
HF@Li ₂₄ F ₂₄ <i>oct-6</i>	2.08	+0.29 (+16%)	-201[+67]
H ₂ O@Li ₃₆ F ₃₆ <i>dod-6</i>	1.14	-0.66 (-37%)	-517[-120]
HF@Li ₃₆ F ₃₆ <i>dod-6</i>	1.22	-0.56 (-31%)	-573[-59]
H ₂ O@C ₆₀ nanocage	0.52	-1.34 (-72%)	-554[+9]
HF@C ₆₀ nanocage	0.52	-1.26 (-71%)	-479[-64]
H ₂ O@B ₃₆ N ₃₆ nanocage	1.17	-0.69 (-37%)	-547[-84]
HF@B ₃₆ N ₃₆ nanocage	1.09	-0.69 (-39%)	-374[-63]
H ₂ O@Be ₃₆ O ₃₆ nanocage	1.61	-0.25 (-13%)	-535[-187]
HF@Be ₃₆ O ₃₆ nanocage	1.63	-0.15 (-8%)	-322[-97]
H ₂ O@Li ₃₆ F ₃₆ nanocage	2.20	+0.34 (+18%)	-152[-76]
HF@Li ₃₆ F ₃₆ nanocage	2.13	+0.35 (+20%)	-100[-59]

Table 3: Electronic dipole moment (along the nanotube axis) μ of endohedral complexes with H₂O or HF molecule inside; $\delta\mu$ denotes the change of the dipole moment of the endohedral complex with respect to those computed for the encapsulated H₂O and HF molecules when they are isolated (1.80 and 1.79 D, respectively). E_{bind} is the binding energy of endohedral complexes. *oct-x* and *dod-x* denote octagonal or dodecagonal transversal section with $x=5,6,7$ layers.

system	μ (D)	$\delta\mu$ (D)	E_{bind} (meV)
H ₂ O@Li ₂₀ F ₂₀ <i>oct-5</i>	2.07	+0.27 (+15%)	-193
H ₂ O@Li ₂₄ F ₂₄ <i>oct-6</i>	2.43	+0.63 (+35%)	-230
H ₂ O@Li ₂₈ F ₂₈ <i>oct-7</i>	2.36	+0.56 (+31%)	-228
HF@Li ₂₀ F ₂₀ <i>oct-5</i>	1.40	-0.38 (-21%)	-183
HF@Li ₂₄ F ₂₄ <i>oct-6</i>	2.08	+0.29 (+16%)	-201
HF@Li ₂₈ F ₂₈ <i>oct-7</i>	1.68	-0.11 (-6%)	-204
H ₂ O@Li ₃₀ F ₃₀ <i>dod-5</i>	1.37	-0.43 (-24%)	-578
H ₂ O@Li ₃₆ F ₃₆ <i>dod-6</i>	1.14	-0.66 (-37%)	-517
H ₂ O@Li ₄₂ F ₄₂ <i>dod-7</i>	1.28	-0.52 (-29%)	-265
HF@Li ₃₀ F ₃₀ <i>dod-5</i>	1.05	-0.74 (-41%)	-592
HF@Li ₃₆ F ₃₆ <i>dod-6</i>	1.22	-0.56 (-31%)	-573
HF@Li ₄₂ F ₄₂ <i>dod-7</i>	1.20	-0.59 (-33%)	-168

Table 4: Energy barrier (in eV) for the encapsulation of H₂O and HF molecules in selected nanotubes.

system	energy barrier (eV)
H ₂ O@C ₉₆ (4,4)	0.470
HF@C ₉₆ (4,4)	0.121
H ₂ O@C ₁₂₀ (5,5)	0.000
HF@C ₁₂₀ (5,5)	0.000
H ₂ O@B ₄₈ N ₄₈ (4,4)	0.287
HF@B ₄₈ N ₄₈ (4,4)	0.062
H ₂ O@Be ₄₈ O ₄₈ (4,4)	2.573
HF@Be ₄₈ O ₄₈ (4,4)	3.733
H ₂ O@Ga ₄₈ N ₄₈ (4,4)	2.501
HF@Ga ₄₈ N ₄₈ (4,4)	1.703
H ₂ O@Li ₂₄ F ₂₄ <i>oct-6</i>	0.499
HF@Li ₂₄ F ₂₄ <i>oct-6</i>	0.412
H ₂ O@Li ₃₆ F ₃₆ <i>dod-6</i>	0.000
HF@Li ₃₆ F ₃₆ <i>dod-6</i>	0.000

the sum of the dipole moments of isolated H_2O and HF molecules (+43%) and also of the dipole moment of the isolated H_2O - HF complex (+11%).

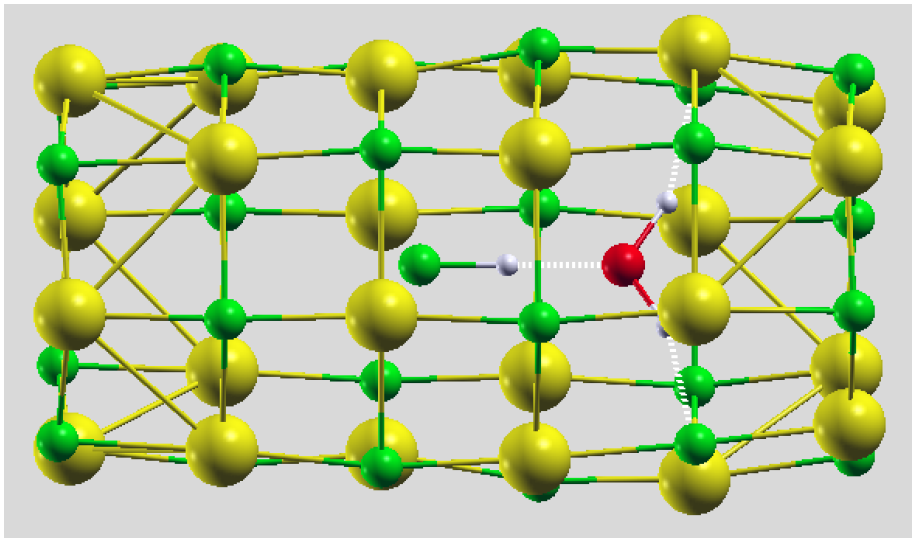


Figure 11: $\text{HF-H}_2\text{O}@Li_{24}F_{24}oct-6$ endohedral nanostructure (longitudinal view). Yellow, green, red, and white balls represent Li, F, O, and H atoms, respectively. White dashed lines indicate Hydrogen bonds.

Conclusions

We have presented the results of a first-principles study of screening effects in endohedral complexes made up of small molecules, with a finite electronic dipole moment, encapsulated into different nanotubes. A detailed analysis of the effective dipole moment of the complexes and of the electronic charge distribution suggests that screening effects crucially depend not only on the nature of the intramolecular bonds but also on the size and the shape of the nanotubes and on the specific encapsulated molecule. As observed in endohedral nanocages, screening is maximum in covalent-bond carbon nanotubes, while it is reduced in partially-ionic nanotubes and an antiscreening effect is observed in some ionic nanotubes. However in this case the scenario is more complex than in corresponding ionic nanocages. In fact the specific geometric structure of alkali-halide, ionic nanotubes turns out to be crucial for determining the screening/antiscreening behavior: while nanotubes with octagonal transversal

section can exhibit an antiscreening effect, which quantitatively depends on the number of layers in the longitudinal direction, instead nanotubes with dodecagonal section are always characterized by a reduction of the total dipole moment, so that a screening behavior is observed. The antiscreening effect in octagonal nanotubes is particularly pronounced for the encapsulated water molecule or the HF-H₂O chained molecule, characterized by the formation of Hydrogen bonds. A detailed structural and electronic analysis has been carried out to elucidate the occurrence of screening/antiscreening effects in different nanotubes. Our results show that, even in nanotube structures, one can tune the dipole moment and generate electrostatic fields at the nanoscale without the aid of external potentials. We can also expect some transferability of the observed screening/antiscreening effects in other nanostructures and 2D materials.

Acknowledgements

We acknowledge funding from PARD-2024, relative to the project “Ab initio study of dielectric properties of innovative nanostructures”. Moreover, this work is supported in part by the MUR Departments of Excellence grant 2023-2027 ”Quantum Frontiers” paradigm for the control of Nanoscale Phenomena”.

References

- (1) Kroto, H. W.; Heath, J. R.; O’Brien, S. C.; Curl, R. F.; Smalley, R. E. C₆₀: Buckminsterfullerene. *Nature* **1985**, *318*, 162.
- (2) Akasaka, T; Nagase, S. *Endofullerenes: A New Family of Carbon Clusters*, Kluwer Academic, Dodrecht, Netherlands, 2002.
- (3) Suetsuna, T.; Dragoe, N.; Harneit, W.; Weidinger, A.; Shimotani, H.; Ito, S.; Takagi, H.; Kitazawa, K. Separation of N₂@C₆₀ and N@C₆₀. *Chem.–Eur. J.* **2002**, *22*, 5079.
- (4) Komatsu, K.; Murata, M.; Murata, Y. Encapsulation of molecular hydrogen in fullerene C₆₀ by organic synthesis. *Science* **2005**, *307*, 238.
- (5) Kurotobi, K.; Murata, Y. A Single Molecule of Water Encapsulated in Fullerene C₆₀. *Science* **2011**, *333*, 613.
- (6) Bloodworth, S. *et al.* First Synthesis and Characterization of CH₄@C₆₀. *Angew. Chem., Int. Ed.* **2019**, *58*, 5038.
- (7) Jaworski, A.; Hedi, N. Local energy decomposition analysis and molecular properties of encapsulated methane in fullerene (CH₄@C₆₀). *Phys. Chem. Chem. Phys.* **2021**, *23*, 21554.

- (8) Sinha, S.; Sanfo, K.; Dallas, P.; Kumar, S.; Porfyraakis, K. Process Parameter Optimisation for Endohedral Metallofullerene Synthesis via the Arc-Discharge Method. *Inorganics* **2024**, *12*, 38.
- (9) Ramachandran, C.; Sathyamurthy, N. Water clusters in a confined nonpolar environment. *Chem. Phys. Lett.* **2005**, *410*, 348.
- (10) Yagi, K.; Watanabe, D. Infrared spectra of water molecule encapsulated inside fullerene studied by instantaneous vibrational analysis. *Int. J. Quant. Chem.* **2009**, *109*, 2080.
- (11) Ensing, B.; Costanzo, F.; Silvestrelli, P. L. On the Polarity of Buckminsterfullerene with a Water Molecule Inside. *J. Phys. Chem. A* **2012**, *116*, 12184.
- (12) Silvestrelli, P. L.; Subashchandrabose, S.; Seif, A.; Ambrosetti, A. Screening and antiscreening in fullerene-like cages: Dipole-field amplification with ionic nanocages. *Carbon Trends* **2023**, *10*, 100242.
- (13) Fernandez-Lima, F. A.; Henkes, A. V.; da Silveira, E. F.; Chaer Nascimento, M. A. Alkali Halide Nanotubes: Structure and Stability. *J. Phys. Chem. C* **2012**, *116*, 4965.
- (14) Mussi, V.; Granone, F.; Boragno, C.; Buatier de Mongeot, F.; Valbusa, U.; Marolo, T.; Montoreali, R. M. Surface nanostructuring and optical activation of lithium fluoride crystals by ion beam irradiation. *Appl. Phys. Lett.* **2006**, *88*, 103116.
- (15) Kim, Y. Power-law-type electron injection through lithium fluoride nanolayers in phosphorescence organic light-emitting devices. *Nanotechnology* **2008**, *19*, 355207.
- (16) Giannozzi, P. *et al.* QUANTUM ESPRESSO: a modular and open-source software project for quantum simulations of materials. *J. Phys.: Condens. Matter* **2009**, *21*, 395502.
- (17) Sabatini, R.; Gorni, T.; de Gironcoli, S. Nonlocal van der Waals density functional made simple and efficient. *Phys. Rev. B* **2013**, *87*, 041108(R).

- (18) Vydrov, O. A.; Van Voorhis, T. Nonlocal van der Waals density functional: The simpler the better. *J. Chem. Phys.* **2010**, *133*, 244103.
- (19) Silvestrelli, P. L.; Ambrosetti, A. van der Waals corrected DFT simulation of adsorption processes on transition-metal surfaces: Xe and graphene on Ni(111). *Phys. Rev. B* **2015**, *91*, 195405.
- (20) Silvestrelli, P. L.; Ambrosetti, A. Van Der Waals-Corrected Density Functional Theory Simulation of Adsorption Processes on Noble-Metal Surfaces: Xe on Ag(111), Au(111), and Cu(111). *J. Low. Temp. Phys.* **2016**, *185*, 183.
- (21) Perdew, J. P.; Burke, K.; Ernzerhof, M. Generalized Gradient Approximation Made Simple. *Phys. Rev. Lett.* **1996**, *77*, 3865.
- (22) Zhang, K.; Stocks, G. M.; Zhong, J. Melting and premelting of carbon nanotubes. *Nanotechnology* **2007**, *18*, 285703.
- (23) Dietel, J.; Kleinert, H. Lindemann parameters for solid membranes focused on carbon nanotubes. *Phys. Rev. B* **2009**, *79*, 075412.
- (24) Dolgonos, G. A.; Peslherbe, G. H. Encapsulation of diatomic molecules in fullerene C₆₀: implications for their main properties. *Phys. Chem. Chem. Phys.* **2014**, *16*, 26294.
- (25) Henkelman, G.; Uberuaga, B. P.; Jonsson, H. A. Climbing image nudged elastic band method for finding saddle points and minimum energy paths. *J. Chem. Phys.* **2000**, *113*, 9901.